# Cleaning Sky Survey Databases using Hough Transform and Renewal String Approaches

A. J. Storkey[1,2], N. C. Hambly[2], C. K. I. Williams[1], R. G. Mann[2,3]
[1] *School of Informatics, University of Edinburgh, Forrest Hill, Ediburgh EH1 2QL.*
[2] *Institute for Astronomy, University of Edinburgh, Blackford Hill, Edinburgh, EH9 3HJ*
[3] *National E-Science Centre, South College Street, Edinburgh, EH8 9AA.*

Accepted —. Received —; in original form —

**ABSTRACT**

Large astronomical databases obtained from sky surveys such as the SuperCOSMOS Sky Survey (SSS) invariably suffer from spurious records coming from artefactual effects of the telescope, satellites and junk objects in orbit around earth and physical defects on the photographic plate or CCD. Though relatively small in number these spurious records present a significant problem in many situations where they can become a large proportion of the records potentially of interest to a given astronomer. Accurate and robust techniques are needed for locating and flagging such spurious objects, and we are undertaking a programme investigating the use of machine learning techniques in this context. In this paper we focus on the four most common causes of unwanted records in the SSS: satellite or aeroplane tracks, scratches, fibres and other linear phenomena introduced to the plate, circular halos around bright stars due to internal reflections within the telescope and diffraction spikes near to bright stars. Appropriate techniques are developed for the detection of each of these. The methods are applied to the SSS data to develop a dataset of spurious object detections, along with confidence measures, which can allow these unwanted data to be removed from consideration. These methods are general and can be adapted to other astronomical survey data.

**Key words:** astronomical databases: miscellaneous – catalogues – surveys – methods: data analysis – statistical

## 1 INTRODUCTION

Sky surveys in astronomy are a fundamental research resource (Banday et al. 2001). Surveys form the basis of statistical studies of stars and galaxies, enabling work ranging in scale from the solar neighbourhood to a significant fraction of the observable universe. Surveys are carried out in all wavelength ranges, from high energy gamma rays (Paciesas et al. 1999) to the longest wavelength radio atlases (Bock et al. 1999). Despite this diversity, there are certain features common to most digital surveys: pixel images at a given spatial and spectral resolution are processed using a pixel analysis engine to generate lists of object detections containing parameters describing each detection. In most cases, the object detection algorithm has to be capable of finding a heterogeneous family of objects, for example point–like sources (stars, quasars); resolved sources (e.g. galaxies) and diffuse, low surface–brightness, extended objects (e.g. nebulae). Object parameters describing each detection typically include positions, intensities and shapes. The volume of pixel data required to be processed necessitates totally automated pixel processing, and of course no imaging system is perfect. These facts (imperfect image recording and automated, generalised pixel processing) lead to the problem of spurious object catalogue records in all sky survey databases, although the exact nature of the spurious objects varies. For example, direct digital sky surveys suffer less from satellite tracks (though they do exist) because of the short exposure time needed for charge coupled device (CCD) arrays compared with photographic plates. In fact because the satellite tracks tend to be significantly shorter, they are harder to detect using standard approaches making the developments in this paper more rather than less important. Infra-red surveys are likely to suffer less from satellite track problems as the tracks will be a couple of orders of magnitude fainter in the near-infra-red than in the optical. However it is still likely that some will be detectable, even if in smaller numbers. Optical artefacts from telescope design occur independent of the digitisation method.

This paper looks at a class of problems which are the most significant sources of unwanted records in the SuperCOSMOS Sky Survey (SSS) data. The SSS is described in a series of papers (Hambly & et al 2001 and references therein). Briefly, the SSS consists of Schmidt photographic plates scanned using the fast, high precision microdensitometer SuperCOSMOS (e.g. Hambly et al. 1998). The survey is made from 894 overlapping fields in each of three colours (blue, red and near–infrared denoted by the labels J, R and I respectively); one colour (R) is available at two epochs to provide additional temporal information. Each image contains approximately $10^9$ 2-byte pixels. The pixel data from each photograph in each colour and in each field are processed into a file of object detections; each object record contains parameters describing that object. The SuperCOSMOS pixel analyser is described in Hambly et al. (2001) and references therein. Also described are some classification and quality flags that are derived for each object detection, and the deblending algorithm which attempts to unscramble groups of close or merged objects. Presently, the entire southern hemisphere is covered, primarily using plates from the UK Schmidt Telescope. Data and many more details are available online at `http://www-wfau.roe.ac.uk/sss`.

SSS data take the form of pixel images and object catalogues derived from them. The SSS database is, like any other astronomical database, subject to the limitations of its imaging system and pixel processing engine. The SSS object catalogues are therefore contaminated by spurious object records. The types of spurious objects fall into three broad classes:

- Linear features: Satellite tracks, aeroplane tracks, fibres left on the plates during digitisation and scratches on the emulsion all produce linear features with varying curvature characteristics and lengths. Scratches and fibres tend to be short. Satellite tracks can be short or long for a variety of reasons. Aeroplane tracks usually traverse the plate but often consist of dashed sections corresponding to a flashing light. Spinning satellites can also caused dashed tracks.
- Near-circular elliptical optical artefacts around bright stars due to the internal reflections within the telescope.
- Diffraction spikes: linear features which are located (almost) horizontally and (almost) vertically on the plate in the region of bright stars.

How these features translate into objects in the sky survey catalogue depends also on the approach of the program which processes the digital picture into object catalogue records. For the SuperCOSMOS Sky Survey many of the largest linear features or parts of linear features are clearly non–astronomical in origin, cannot be processed by the pixel analyser, and therefore do not give rise to spurious object catalogue records. The rest tend to be represented in the catalogue as a number of objects lying along a line. Hence even if a track traversed the whole plate in the original image, in the derived catalogue data it might only translate into a set of objects traversing a short section of the original track.

The focus of this paper is on locating objects in an astronomical dataset derived from or affected by the characteristics listed above, and distinguishing them from true astronomical objects. Because much work has usually already been done deriving the object data from images, because in many cases original image data may not be available, and because of the huge size of the images involved, we are not considering working with the images directly, only with the derived datasets.

The paper continues with Section 2, giving further detail of the different sorts of spurious data which might be encountered. Some standard image processing techniques from the computer vision community are introduced in Section 3, along with an assessment of how appropriate they are for problems of this paper. It turns out that more accurate and informative methods can be made available. The method of renewal strings (Storkey et al. 2003) has been developed for overcoming the difficulties of the standard approaches, and is ideally suited for detection of satellite tracks, scratches and other linear phenomena. It is a Bayesian probabilistic method, and so also provides some confidence measures for the classification. Renewal strings are described in Sections 4 and 5. Their use is elaborated in Section 6. The results of applying these different methods are shown in Sections 7 through to 9 along with some analysis of performance. Evaluation of the results is given in Section 10. In conclusion, information on how these results have been made available for the SSS data, along with discussion of further work in this area and of the reciprocal benefits of this work to the machine learning community can be found in Section 11.

## 2 SPURIOUS OBJECTS IN ASTRONOMICAL DATA

A number of distinct classes of spurious object commonly occur in optical/ near-infrared sky survey data. The descriptions given here refer to the form they take within the SSS data. However many other astronomical databases have similar characteristics.

### 2.1 Satellite Tracks

Satellite Tracks are due to movement of the satellite over the duration of exposure for a given field. They follow paths which are almost straight elliptic sections. Movement into or out of the Earth's shadow, the two ends of exposure, or removal by the object recogniser can all stop the data related to a satellite track from traversing the whole plate. The positions of satellite tracks are unpredictable, and using a (probably incomplete) catalogue of satellites and orbiting debris would be a complicated and probably unreliable way of locating them. The data related to satellite tracks can vary considerably. For some narrow and faint tracks the data can be sparsely distributed along the track. For bolder tracks the data might consist of objects with ellipses aligned along the track. Sometimes the data take the form of very dense circular objects. Figure 1 gives two examples of satellite tracks on the SuperCOSMOS Sky Survey plates and the resulting data derived from them.

### 2.2 Aeroplane Tracks

Aeroplane tracks arise from aeroplane lights as they cross the field of view. Often (but not always) the lights are flashing and so dashed tracks are seen. All the representational issues which apply to satellite tracks also apply to the data derived from aeroplane lights. Examples can be seen in Figure 2.

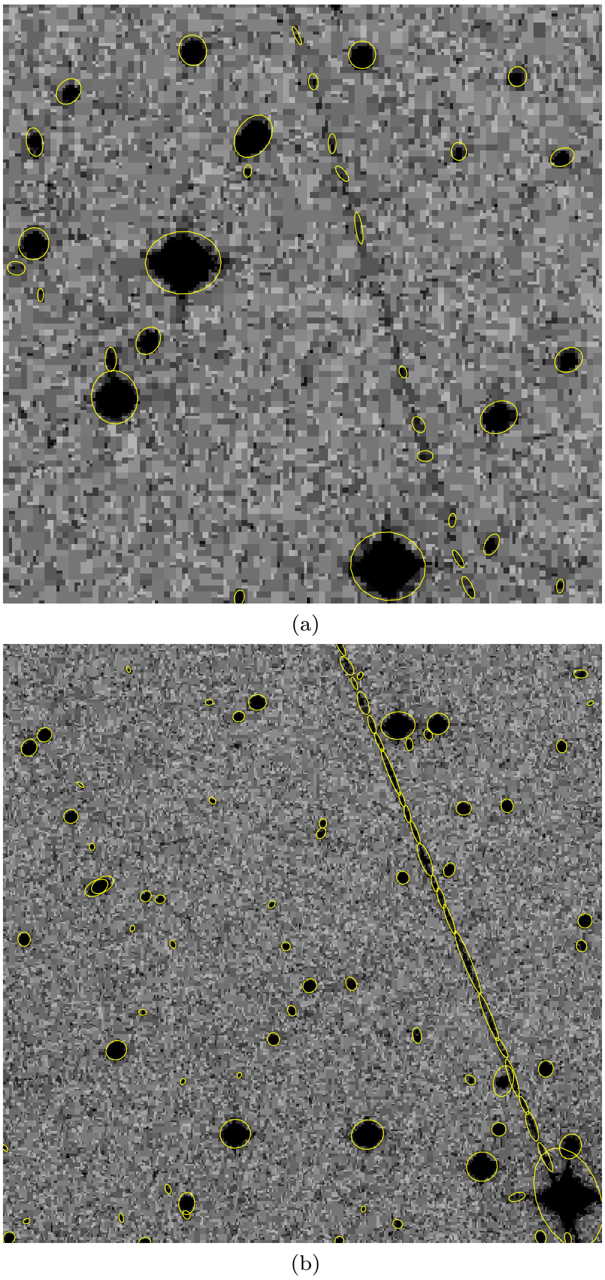
(a)

(b)

**Figure 1.** (a) and (b): Two tracks seen close up. Extracted data is shown as ellipses superimposed on the digitised image. (a) A faint satellite track with sparse spurious objects distributed along it. (b) A denser track with spurious objects elongated along the track. The 'blocky' appearance of the sky pixels is a result of them having passed through a Haar–transform compression algorithm.

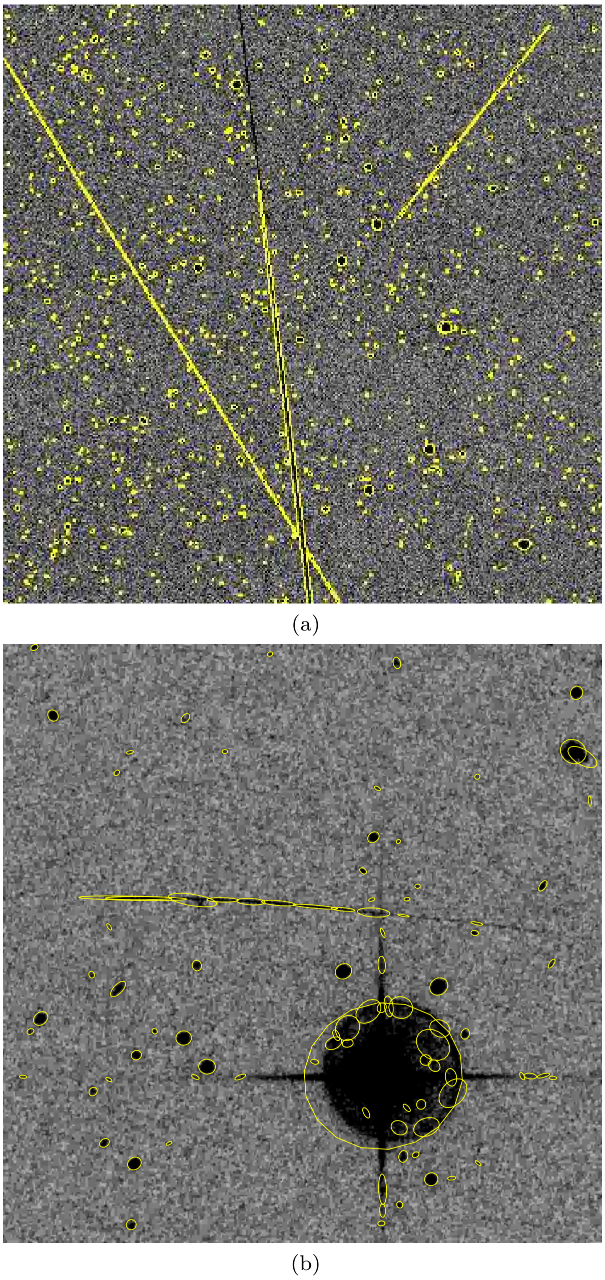
(a)

(b)

**Figure 2.** (a) A number of aeroplane tracks in field UKJ413: the most vertical is a very solid aeroplane track, which has been converted into very large elliptical objects. Some of the objects corresponding to this track were too large for pixel analysis and hence are effectively removed. The second (sloping left) is a solid track converted into a large number of small objects lying along the track. The third is one section of a dashed aeroplane track corresponding to flashing lights. (b) A small slightly curved scratch. Scratches are often longer, fainter or more curved than this, but small scratches are also common.

### 2.3 Scratches

Scratches on the plate surface are not uncommon despite all the effort taken to protect the emulsion from such. These scratches can be seen by the SuperCOSMOS digitiser as darker regions and hence are confused with photographic exposure. They are usually (but not always) short, they tend to be curved, and sometimes the curvature can vary significantly along the scratch. Again the same issues occur in translating these linear features into data. An example of a scratch can be seen in Figure 2.

### 2.4 Dust fibres

Fibres from clothing which contaminate the plate during scanning are not a large problem in the original SSS data, but are a noticeable problem in the SSS H–alpha survey, despite 'clean room' operating conditions for the SuperCOSMOS measuring machine. This is because the original photographic medium for the latter is film rather than glass, and film is more prone to electrostatic attraction of particles. Although some of the features of fibres can be removed by the methods developed here, many of the very small tangled fibres of the H alpha survey would not be detected. Although they are strictly one-dimensional features they tend to have many discontinuities in their first derivative. They are often small, and the combination of these effects mean they might only result in a few unaligned objects in the derived dataset. Many of these fibres might be hard to locate without going back to the original image data. See Figure 3 for an example.

### 2.5 Stellar Halos

Because survey observations are optimised for faint objects, bright stars and galaxies can often have annoying optical artefacts associated with them. The halos around bright stars are the first of these which we will be considering. These halos come from internal reflections within the telescope and take a number of forms. First there is an area of brightness directly surrounding a bright star, decaying with distance away from the star centre. Second there could be a smaller uniform disc around the star which is more exposed than the background. In the centre of a plate this disc will be centred at the star, but at the edges it could be offset from the centre. This disc could have an outer edge which is more exposed than the disc itself. Outside this inner disc there might be another outer disc. This will be larger than the inner disc and centred further from the star than the centre of the inner disc. Once again this disc could have a more exposed outer edge. It is theoretically possible to have further discs, but these are only occasionally observed. The discs are elliptical.

When images containing these halo artefacts undergo pixel analysis, there are generally two types of spurious record that are produced. First there is a high density of erroneous detections in the vicinity of the bright star corresponding to the immediate bright area surrounding the star, or in the region of the inner disc. Second there can be a ring of object detections following the edge of either or both of the inner and outer discs. Examples of this are seen in Figure 3.

### 2.6 Diffraction Spikes

Diffraction spikes are also associated with bright objects. They are almost horizontal and almost vertical lines emanating from the bright star which are due to diffraction about the telescope struts. The size and length of the diffraction spikes is dependent on the brightness of the star: brighter stars produce longer diffraction spikes. The deviation of the lines from the horizontal and vertical is related to the position on the plate. Once again greater deviations occur further from the field centre.

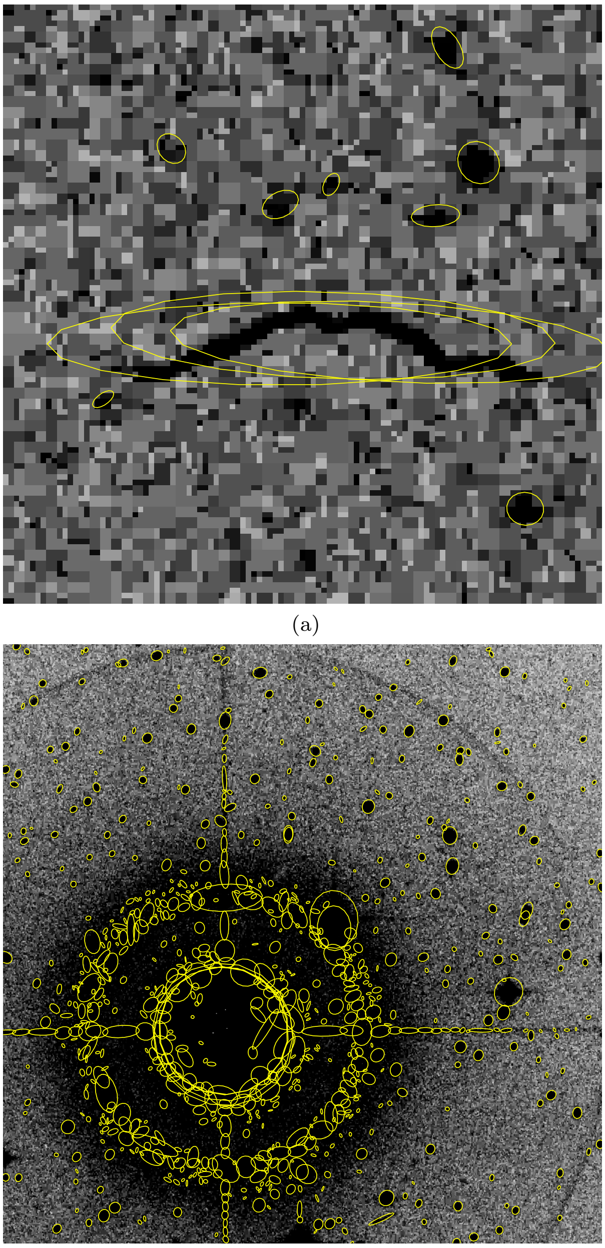

(a)

(b)

**Figure 3.** (a) A small fibre on a plate resulting in 3 spurious objects. It would be hard to detect these on database information alone. (b) A large bright star on UKR005. the diffraction spikes and halos, along with their data counterparts are clear. An outer halo is also evident, but in this case it is too faint to have caused any detections.

Because the SuperCOSMOS image analyser fits ellipses to objects, spurious objects in the dataset along the line of the diffraction spikes often have ellipses aligned along (or occasionally perpendicular to) the diffraction spike. Examples are given in Figure 3.

### 2.7 Other Detritus

The vast majority of spurious objects fall into the above classes. However other problems such as defects in the plate emulsion can produce spurious objects in the dataset. Also small defects may not be detectable from only the catalogue data alone and so it might be necessary to return to the original images. This paper deals only with detecting spurious records from catalogue data.

### 2.8 Problems Caused by Spurious Objects

Spurious objects will introduce errors in statistical results derived from the data, and make locating particular classes of objects much harder. The fainter tracks result in many spurious, elliptical low surface brightness 'galaxies' contaminating the respective object catalogue. A single–colour galaxy catalogue, created from the UKJ survey for the purposes of studying faint blue galaxies would therefore be highly contaminated by spurious, aligned image records. This could severely impact a statistical analysis of the type described in Brown et al. (2002), where the degree and scale of real galaxy alignment is being sought. In order to eliminate this possibility, Brown et al. used a two–colour (JR) paired catalogue, but this of course compromised the depth of the study and also biased it against faint blue galaxies which do not appear on the R plates. Ideally, one might like to perform this study on a single colour (J) galaxy catalogue. In many general problems we may be interested in real objects which might be in one dataset but not in an other. For example, objects which are evident at one wavelength but not at another may be of interest. Fast moving stars will also be in different places in catalogues derived from observations at different times, meaning that they will not have exact positional matches across the datasets, (e.g. Oppenheimer et al. (2001)). Unfortunately satellite track artefacts have the same characteristics, as they will only ever appear (in the same place) in one dataset, and not in any other. Searches on non-matching objects will bring up all the objects of interest *plus* all of these artefacts. When searching for rare objects the spurious records can be overwhelming. Removing spurious objects, then, is of broad importance in astronomy.

## 3 POSSIBLE APPROACHES

There have not been many attempts at tackling the problem of labelling spurious objects derived from satellite tracks, scratches or other linear phenomena despite the ubiquitous nature of the problem and the difficulties these objects produce for many tasks which sky surveys are used for.

### 3.1 Hough Transform

The most obvious way to locate lines of objects in two dimensional data utilises the Hough transform. Indeed in Cheselka (1999) and Vandame (2001) the authors followed this approach. The Hough transform (Hough 1959) is a standard image processing method from which other related approaches have been developed. In its standard form it is generally used in low dimensional situations to find lines containing a high density of points hidden amongst a large number of other points distributed widely across the whole space. Commonly it is used for line detection in images.

The Hough transform works by moving from the space of points to the Hough space, that is the space of lines. Every point $(d, \theta)$ in Hough space corresponds to a line in the original space which is a perpendicular distance $d$ from the centre of the data space and inclined at angle $\theta$ from the vertical.

One method of implementing the Hough transform would search through a finite number of line angles $\theta$. For each angle all the data points would be considered. For each data point we would find the (perpendicular) distance from the origin of the straight line *through* that point at the relevant angle. This distance would then be discretised, and the count in an accumulator corresponding to this discretised distance would be increased by one[1]. The result of this is a count for each angle and each perpendicular distance. Neglecting dependencies between the accumulators at different angles and assuming, as a null hypothesis, a uniform scattering of points[2] in the data space, we know the distribution of the count in a given Hough accumulator will be Poisson with a mean proportional to the length of the corresponding line. If on the other hand there is also a line of high density points in amongst the uniform scattering, then this Poisson distribution will not be the correct model for the Hough accumulator corresponding to this line. In fact the count will be significantly higher than that expected under the null hypothesis. Hence looking at the probability of the actual count under this null hypothesis, and ideally comparing this to an alternative hypothesis based on some prior model of line counts for satellite tracks, will indicate how likely it is that this accumulator corresponds to a satellite track. A surprisingly large number of papers on, and applications of, the Hough transform focus on finding large absolute values contained within the Hough accumulators rather than comparing them with the null distribution. Needless to say that approach is significantly less accurate and powerful and is not to be recommended.

For an SSS dataset derived from field UKJ005, Figure 4a illustrates the Hough transform of the data. In this figure lighter regions correspond to higher accumulator counts. The large scale variation in light and dark regions comes from the square shape of the plate: lines through the centre along a diagonal are longer than off centre or off diagonal lines, and hence will generally contain more stars. It is also possible to see some sinusoidal lines of slightly increased intensity. These are caused by a local cluster of large numbers of objects - either a galaxy or artefacts surrounding a bright star.

The points in Figure 4a which have been circled correspond to points which have an accumulator count much higher than that which would be suggested by the null Poisson model. In fact one of these Hough accumulators combined with its highest count nearest neighbours corresponds to the data illustrated in figure 4b. In this figure the data have been rotated so that the horizontal axis shows the length along the line of the Hough box (the region in data space corresponding to a given accumulator), and the vertical axis corresponds to the much smaller combined width

[1] A concise tutorial/demo of the Hough transform can be found at http://www.storkey.org/hough.html

[2] More formally assuming that points are sampled from a homogeneous Poisson process.

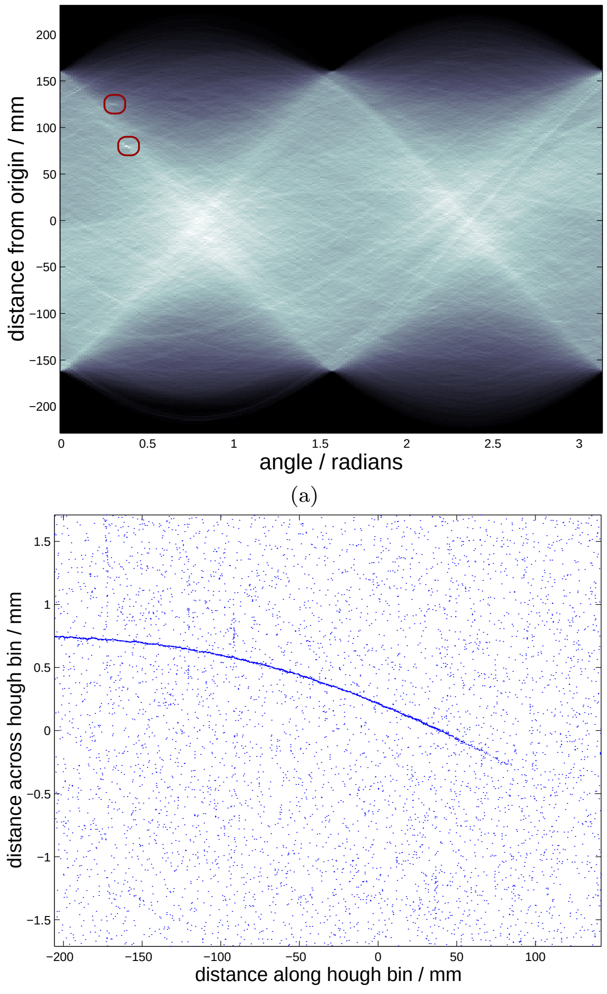

(b)

**Figure 4.** (a) Hough transform of data from field UKJ005. The vertical axis gives the distance from an origin in the centre of the plate (400 bins), the horizontal axis gives the angle of orientation (200 bins). Lighter colours are higher accumulator counts. The circled points are Hough accumulators with a significantly high count, and which correspond to satellite tracks on the plate. The original data which was accumulated in the 3 Hough accumulators at points (0.38,[79 81]) of (a), that is points in the lower circle, is shown in (b). Note the different scales of the two axes. The curvature of the track is obvious from this plot.

of the two neighbouring Hough boxes. The representation shows that this Hough box does indeed contain (part of) a satellite track, in fact the most prominent track on the plate. Part of this track is illustrated in Figure 1(b).

The curved shape of the track gives some hints of the problems which will be encountered when working with satellite tracks. Many real stars and galaxies lie within the the smallest Hough box which could contain the satellite track. Hence flagging everything within the Hough box as possibly spurious will not suffice. Reducing the size of the Hough boxes means that the data from a single track will be split across a number of boxes, and the data within each box might begin to be swamped by the general variations in underlying star and galaxy distribution. This, combined with the fact that some of the tracks and scratches we are interested in locating are very short segments means that the data from the line can be swamped by the random variations in sample density of all the other points along the line. Therefore nonlinear robust fits to the data within Hough boxes are not enough. Add to this the problems of dashed aeroplane tracks and the variable curvature of scratches and it becomes clear that an approach is needed that is more flexible than the Hough transform. Comparisons of the results obtained by the methods developed in this paper and a Hough approach can be found in section 7.

### 3.2 Elliptical Hough Transform

Hough transforms can also be used for features other than straight lines, although more than a few degrees of freedom increases the Hough space which needs to be considered, and for large problems such as these this would quickly become impractical. In fact even a standard circular Hough transform, having three degrees of freedom to the Hough space (centre x coord, centre y coord, radius) would be beyond reasonable computation for large astronomical datasets. However if these degrees of freedom can be constrained then the search space can be reduced to a reasonable size.

In the case of optical halos we know that the elliptical patterns are centred at or near to bright stars, are axis aligned and are near circular. This provides a significant constraint on the centre of the halo which is enough to make an elliptical Hough transform entirely feasible for astronomical data. The details of this particular implementation are given in Section 8. In general, though, the elliptical Hough transform is implemented in much the same way as the linear Hough transform. First we decide on the Hough bin width, denoted $\epsilon$. The parameter set, consisting of deviation from star centre, horizontal radius, and deviation of vertical radius from a circle, are searched through. Each record in the relevant locality is placed in the two accumulators corresponding to the epsilon-width ellipses (with current parameters) which go through that point. Again, after the process is completed, the expected count in each accumulator is Poisson with mean proportional to the area of the corresponding ellipse. A much higher count than that expected from this distribution would correspond to an abnormally high density of points within that ellipse.

### 3.3 RANSAC

RANSAC (Random Sampling and Consensus, Fischler & Bolles 1981) is a robust estimation technique which is used when a large proportion of the data provided is expected to be comprised of outliers. Unlike other robust estimation techniques RANSAC does not use as much data as possible to obtain an initial fit estimate. Rather it chooses a sample of as little data as possible which will determine the required curve (2 points in the case of a straight line). This sampling is repeated as many times as is necessary to ensure that there is a high probability that one sample will obtain no outliers. Each of these samples is then scored by calculating the number of points that are no greater than a given distance $d$ away from the line. An estimate of the line parameters can then be made from these points, or further re-estimation methods can be used.

The RANSAC algorithm is simple. Suppose we are interested in fitting a parametric curve/line with $k$ parameters, and there are $n$ data items. Choose an acceptable probability of failure $P(\text{fail})$. Suppose we expect there are $t$ items which will lie along the curve or line we want to find and fit. The algorithm is

- Repeat $s$ times

(i) Select $k$ data items.
(ii) Fit the curve or line to these $k$ items.
(iii) Calculate the support this curve has (i.e. how many other points lie along the curve).
(iv) Decide whether this curve is to be accepted or rejected dependent on the support.

- End repeat

Under these simple assumptions it is straightforward to show that we need

$$s = \frac{\log P(\text{fail})}{\log(1 - t/n)} \tag{1}$$

to get the required failure probability.

RANSAC is useful in situations where there are a large number of outliers. However the situation presented here is one which exceeds the usefulness of a naive RANSAC application. Given that we might be interested in finding lines of 20 data points in a dataset of 1 million data points, that gives a proportion of 1/50000 of points not considered to be outliers. A naive application of RANSAC would require a sample size $s$ of the order of $(50000)^2$. Furthermore calculating the support for a curve would involve at worst another run through the whole data, making the full cost $o(50000^3)$.

Less naively, a local RANSAC method could be developed. Most tracks are at least piecewise continuous, and it is rare for large regions of tracks to be unrepresented by an object in the catalogue. Recognising, then, that given a true point (a point which is in the track) generally has another true point within its 40 nearest neighbours, say, reduces the required sampling size to an order of $40 \times 50000$. However for each of these samples we would also have to assess the quality of the local support for the points, which would involve the further consideration of about 1000 points in the local area to assess whether they lie along the required line. Presuming we would be happy with a $P(\text{fail}) = 1/100$ (where here this is the probability of detection failure for each *section* of track) this gives a cost of the order of $1 \times 10^{10}$ operations. A very accurate Hough transform considering 1000 different angles will cost about $1 \times 10^9$. Here we have neglected the cost of finding the local neighbours. Again with this RANSAC approach, accurately delineating the ends of a scratch requires further processing, although the more local nature of the algorithm makes it easier. Local density variations can also be included as this form of RANSAC involves local assessment of support. The algorithm will be less accurate in situations where large faint lines occur, as then the line will have to be recognised on the basis of small amounts of local information alone, as there is no way of accumulating information over larger distances. Also focusing on too local a region can cause problems. Objects along a track will deviate from the track a little, and if too short a distance is used to estimate the line of a track, the true track line might never be found to enough accuracy.

In higher dimensions RANSAC becomes much more efficient. The Hough transform scales exponentially with dimensionality, whereas dimensionality is irrelevant for RANSAC. In general this makes RANSAC a more powerful technique.

The renewal strings algorithm of this paper is introduced and implemented in a Hough-like framework. However it is a simple modification to implement it in a RANSAC like framework. In this situation the line angle and positions are chosen by sampling two points (ideally using the local form above), and considering the line through the two points. The rest of the procedure remains the same. With the data in this problem, we would expect the Hough-like and the local RANSAC-like approaches to be the same order of magnitude in terms of cost.

## 3.4 Variations on the Hough transform

The Hough transform has been part of the image processing toolbox for many years, and it would be surprising if adaptations and advances had not been made.

### *3.4.1 Probabilistic Hough Transform.*

That which has become known as the probabilistic Hough Transform (Kiryati et al. 1991) is simply a way of using a subsample of the data to speed things up. It is straightforward to calculate the probability of failing to detect a line that would have been detected if all the data had been used. This can be used to choose an appropriate number of points to subsample.

### *3.4.2 Generalised Hough Transform.*

If the feature to be detected is not easily represented analytically, it might be possible to describe the shape using a lookup table based on a prototype shape. The generalised Hough transform (Ballard 1981) uses this approach.

## 3.5 Related Work

In addition to the work already discussed, there is a fair body of vision literature on robust techniques for line segmentation. For example in Kiryati & Bruckstein (1992) the authors use a smoothing of the Hough accumulator (Hough 1959) to obtain a robust fit. However these approaches tend to be global straight line methods, in the sense that they would not work well for either short line segments or curved lines. In Cheng, Meer and Tyler (Chen et al. 2001), the authors provide methods for dealing with multiple structures which need not cover the whole space. Once again the model deals with straight line fits, and is tested on examples where there is not dominant background data, or large numbers of outliers. Image based techniques for line extraction are common, but tend to be based on continuity considerations, and they are not appropriate in the context where we might be working with data derived from images rather than the images themselves. The important work of Hastie and Stuetzle (Hastie & Stuetzle 1989) on principal curves provides a different direction which does model curved data, but does not provide the robustness and efficiency needed for situations when curves are set in large amounts of other data.

## 4 RENEWAL STRINGS

Renewal strings, first introduced in the machine learning literature in Storkey et al. (2003), are a new probabilistic data mining tool for finding subsets of records following unknown line segments in data space which are hidden within large amounts of other data. The method was developed specifically to address the problem of this paper. Renewal strings combine a model for two dimensional data and a set of models for small numbers of data lying on one dimensional manifolds within the two dimensional space. The design of the model allows efficient line based techniques to be used for separating out the data from the different one dimensional manifolds.

Renewal strings rely on a Bayesian generative approach, and so this section of the paper starts by describing how renewal strings can be used to generate, or simulate, artificial data of the sort we are interested in. Generative models are a probabilistic framework, whereby a prior probability distribution is built that represents belief about what data might be expected. This usually involves forming a model where explanatory hidden (or latent) variables provide a description of the data. The form of this model is such that artificial data can be sampled from the prior distribution.

To use a generative model, it is inverted using Bayes' theorem to provide the posterior distribution over the latent variables given the observed data. This posterior distribution can provide answers to any questions regarding particular explanations for the data. Hence after the renewal strings model is formulated, the same generative model is then inverted using the standard Bayesian formalism to enable the key variables to be inferred from the *real* data. Although this inversion is approximate, it captures the fundamental characteristics of the model.

Renewal strings depend on two tools of probabilistic modelling: the renewal process and hidden Markov models. Hence these two models are introduced here.

### 4.1 Renewal Process Description

One way of modelling points along a line is through renewal processes. A renewal process is a model for event times obtained by defining a probability distribution for the time between events (commonly termed the inter-arrival time). The time at which event $i$ occurs is dependent only on the time of the previous event $i-1$; it obeys the Markov property. The typical example of a renewal process is light bulb failure. The probability that a light bulb is about to fail depends only on how long the light bulb has been burning (the time since the last bulb failed) and not on the life (or any other characteristics) of any of the other light bulbs which had been in the fitting previously. Hence renewal models have the advantage that they are Markovian while at the same time allowing complete flexibility in modelling the inter-arrival times. As we will generally be dealing with one-dimensional spatial concepts rather than temporal ones we will use the term 'inter-point distance' rather than 'inter-arrival time' in the context of this paper.

It is possible that a Markovian model does not capture the major features of a line process, for example a large inter-point distance might be much more likely to be followed by a smaller inter-point distance (a problem characteristic of bus arrival times, for example). The benefits of using a Markovian model, in terms of speed and tractability, led to the decision to focus exclusively on the inter-arrival characteristics of the data and ignore any slight non-Markovian characteristics there might be. If this Markovian model is not good enough then it can be possible to incorporate the non-Markovian elements into the hidden Markov part of the renewal string model, described in the next section.

### 4.2 Hidden Markovian Dynamics

Hidden Markov Models (HMMs) are a ubiquitous tool, seen in many different applications. Almost all speech recognition systems use a hidden Markov model framework. They have also been found to be a vital tool in gene sequence analysis, computer vision, time series prediction and natural language processing. A standard introduction to hidden Markov models can be found in Rabiner (1989). In this section we show how a hidden Markov model can be used to combine a number $m$ of different sorts of satellite tracks or processes together into a switching system.

Suppose we are given an inter-point distance $\Delta t_i$ at a point $i$ and given prior renewal models for the $m$ different types of satellite track processes. Then given a prior probability of a point being part of a particular type of satellite track, we can obtain a posterior probability that the inter-arrival time was characteristic of a particular type satellite track:

$$P(X_i|\Delta t_i) = \frac{P(\Delta t_i|X_i)P(X_i)}{\sum_{X_i} P(\Delta t_i|X_i)P(X_i)}, \tag{2}$$

where $X_i$ labels the type of process ($1, 2, \ldots, m$ for the different types of satellite track).

The problem with this is that the prior probability of a point being part of a satellite track will be highly dependent on whether the last point in the line was part of the same type of satellite track or not. Hence we need some prior model for satellite track continuity. This is most easily defined using a Markov model for the track labels $X_i$. Because $X_i$ are not observable the whole model is called a hidden Markov model.

We introduce a set of conditional transition probabilities $P(X_i|X_{i-1})$ for the change in label between object $i-1$ and object $i$ along the line. We also allow a transition $P(X_i = 0|X_{i-1})$ where $X_i = 0$ denotes the end of the line. The belief network for this system is illustrated in Figure 5. In a belief network, each node represents a random variable, and each directed edge is a direct probabilistic dependence. Hence a belief network is an implicit representation of the conditional independence structures in a distribution. The nodes directly upstream from a given node are called the parents of that node. For each node $V$ a conditional distribution $P(V|\text{Parents of } V)$ needs to be defined. The joint probability distribution over all the nodes is simply the product of the conditional distributions for each node. For more details on belief networks see e.g. Castillo et al. (1997). Probability models which can be represented as belief networks

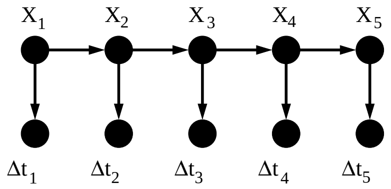

**Figure 5.** Belief network for the hidden Markov renewal process.

without undirected cycles have the advantage of allowing efficient exact inference to be done using belief propagation (Pearl 1988).

The combination of renewal processes and hidden Markov models, henceforth called renewal process hidden Markov models is not new within temporal settings. It has been used for (amongst other things) modelling the pecking behaviour of pigeons (Otterpohl et al. 2000)! Also, in the case that the renewal processes are all Poisson processes, there is a direct relationship between the Renewal Process hidden Markov model and the Markov modulated Poisson process (Scott & Smyth 2003).

### 4.3 Other Variables

Though the positions of the objects will play the most important part in the characterisation of line processes, other characteristics of the data might well be able to contribute to the classification. For example, in satellite tracks, the object ellipses tend to be aligned along the track.

We can modify the hidden Markov model to include input units to $X_i$ relating to any other data fields associated with each point. This produces an obvious generalisation to the hidden Markov model, known as an input-output hidden Markov model (Bengio & Frasconi 1996). Specifically we include elliptical alignment information in the model.

## 5 RENEWAL STRING GENERATION

One way to visualise the complete renewal string model involves building a background image of the stars and galaxies. Having decided on the number and location of the satellite tracks, and the type of each, we thread beads onto a string for each satellite track, where the distances between the beads are defined by the hidden Markov renewal process, stopping when we get $X_i = 0$ in the hidden Markov model. Then we place the beads down on to a background image, keeping the string tight. The final data consists of the positions of the stars and galaxies in the background model, combined with the positions of the beads.

More formally, the Renewal String generative model is built as follows. First 2 dimensional star and galaxy positions are generated from a background spatial model. This could be any spatial process such as an inhomogeneous Poisson process. For the purposes of this paper we define the background model to be a Poisson process which is homogeneous within small regions, but has different rates in different regions. Denote this rate function $\Lambda(\mathbf{r})$ for positions $\mathbf{r}$.

Track processes are superimposed on the background data, to simulate satellite tracks or scratches. There are potentially a number of different track classes, each with different inter-point distributions. The tracks are generated as follows:

- For each $\theta$ from a large but finite set of angles $\Theta$, and for each of a finite set of lines $L$ at that angle, each of a given (narrow) width $w$, a renewal process HMM is used to generate track data.

The renewal process hidden Markov model along the line is implemented using this procedure:

- Along each line, a Poisson process (with large mean inter-point distance $\gamma$) is used as a *birth* process for the track; an event in this process signifies the start of the track generation.
- The class of the track is chosen from the prior distribution $P(X_0)$, and track points are sampled by generating from a renewal process HMM: the inter-point distance is sampled from $P(\Delta t_i|X_i)$ conditioned on the current class, and a new point $t_{i+1}$ is placed the distance $\Delta t_i$ away from the current point, at angle $\theta$ from that point. Then the next class is chosen from the transitions $P(X_{t+1}|X_t)$.
- We stop generating the track either when the edge of the plate is reached or the hidden Markov chain transitions into the 'stop' class. The transition into the stop class initiates the birth process again, which allows more than one track to be generated along the same line.
- Each point in each track is independently perturbed perpendicular to the line of the track uniformly across the track width $w$.

Note that it is possible for a track to be turned on before reaching the region of interest (in this case the plate edge), but not yet be turned off, and hence the track will start at the edge of the plate. As the birth process produces rare events most lines will not contain any tracks at all.

The set of angles $\Theta$ is generally chosen to be regularly spaced between 0 and 180 degrees, and the lines $L$ are chosen to cover the region of consideration with a 2 line overlap; each point in the space lies in 2 and only 2 lines at a given angle.

Figure 6 illustrates a sample from a generative model of this form. We see a background model, along with two different types of tracks, one of which is a high density broken line, the other a medium density line. The model only generates straight line segments. Curves can be approximated using piecewise linear segments.

## 6 INFERENCE AND LEARNING

The generative Renewal String model says how to simulate background data and the data corresponding to different tracks from a given parameter set. These two elements can then be combined to form the final observable data. What we are interested in is the inverse model: how to separate the background and track records given the whole data and a particular set of parameters. This inverse is given by Bayes theorem:

$$P(X|D, \Phi) = \frac{P(D|X, \Phi)P(X|\Phi)}{P(D|\Phi)} \qquad (3)$$

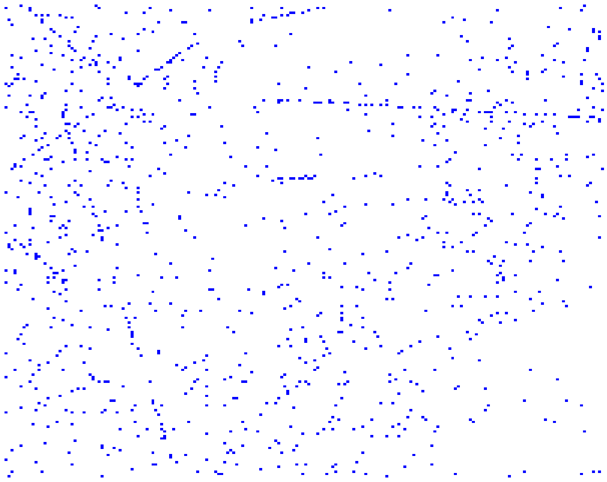

**Figure 6.** A sample from a 3 hidden-state renewal strings prior, illustrating a background model, and 7 lines with differing characteristics.

where $D$ denotes the data, $X$ a set with each element labelling whether a point corresponds to a star/galaxy or one of the different types of track. $\Phi$ is presumed to be a known set of parameters.

We require a reasonably fast inference scheme for this model. Borrowing from the Hough transform approach it could be sensible to resort to line-based techniques in order to perform inference. The Hough transform looks through a comprehensive set of lines in the data, and finds those with a high accumulator. To implement the renewal string we take this one step further. Rather than just count the points along the line, a renewal process HMM is run along the line to find points which could be best classified as part of a track. This approach is only an approximate inference scheme for the aforementioned generative model. The main issue is that, as with the Hough transform, the dependence between lines at different angles is ignored. The inference scheme for a single line is exact in the case where data from all tracks other than those along that line have been removed. In reality, though, such data remains. However because there are few tracks, tracks at other angles will contribute at most a small number of points to the data along the current line, and so this is likely to have limited effect on the inference for the current line. This is the primary approximation assumption of the inference method.

To work with lines rather than with spatial variables, we use the fact that a spatial point distribution which is an inhomogeneous Poisson process will correspond to an inhomogeneous Poisson process along the length of any line (with some given width) going through that region of space. Hence when we condition on the fact that we are considering one particular line, a one dimensional Poisson process can be used instead of a spatial one. The inhomogeneity of the Poisson process takes care of the fact that the background model is not likely to take the same form across the whole plate.

Suppose we have an estimate for the density $D_b$ of background objects local to each point. The full initialisation and inferential process can now be given. As stated above, $\Theta$ gives the set of angles to be considered (from 0 to 180 degrees), and $L = L(\Theta)$ the set of lines at each angle:

```
1) Set the line width $w$ based on the expected maximum width of the lines to be found. Define the inter-point distance distribution $P(\Delta t|X, D_b)$ for each class $X$ including the background class. This can depend on the background object density at that point. Define the class transition probabilities $P(X_i^k|X_{i-1}^k)$ and initial probabilities $P(X_0^k)$.
2) For each angle $\theta$ from the set $\Theta$
    a) For every point in the dataset, find all the lines $L'$ of width $w$ in $L$ which contain the point. Store the position $t$ along each line in $l'$ in a bin corresponding to that line.
    b) For each line in $L$, sort all the distances in its bin. Use these distances as the data for an HMM with emission probabilities $P(\Delta t|X, D_b)$ and transition probabilities $P(X_i^k|X_{i-1}^k)$. Run the usual forward-backward inference (see Appendix A) to get marginal posterior class probabilities for each point. Flag any points which have a low probability of being background objects and note the angle at which these points were detected.
3) End for
```

At the end of this process, the flagged points are the points suspected to be part of a track or scratch. The associated probability gives extra information regarding the certainty of this classification.

Note that, in terms of the generative model, the transition probability out of the background state, $P(X_i^k \neq 0|X_{i-1}^k = 0)$, is given by the probability that the point is generated by the birth process rather than the background process. In practice, at least for this work, we approximate this by a fixed empirically determined value. Then we can take the initial class probability $P(X_0^k)$ as given by the equilibrium distribution of the Markov chain.

To estimate the rate $\Lambda(r)$ of the background inhomogeneous Poisson process, we assume there is a length scale $s$ such that, for regions of size $s \times s$, the contributions from the satellite tracks to the total number of points, and the variation in background star/galaxy density are both negligible. Then the local mean of the background Possion process can be approximately obtained from the total density of points in a local region of size $s \times s$.

Tuning of the parameters could be done with the usual expectation maximisation algorithm for HMMs (Rabiner 1989). On the other hand empirical ground truth estimates could be used to set the parameters. In this work the tracks are also modelled as Poisson processes (a specific form of renewal process with an exponential inter-point distance). The fundamental reason for this is that along the line of a satellite track there will also be objects corresponding to stars and galaxies. The point density along a track from a satellite moving in front of a dense distribution of stars will be higher than one passing in front of a relatively sparse region of sky, and hence the line of objects along each track is a superposition. Poisson processes have the advantage that the superposition of two Poisson processes is a Poisson process. The equivalent statement is not true for more general forms of renewal processes.

### 6.1 Preprocessing using the Hough transform

Although we will show in section 7.1 that a standard Hough transform will not be able to find all the linear features in the data, it is certainly true that it will find the larger satellite tracks and other features that cover a significant distance on the plate. If these larger features were the only ones of significant interest then the Hough transform could be used as a preprocessor to determine which lines should be checked for the features we want. The renewal string algorithm is only run along a particular line if there seems to be enough support obtained from the number of objects along that line. In this sense renewal strings are a complement to the Hough transform rather than an alternative.

## 7 DETECTIONS OF SATELLITE TRACKS, AEROPLANE TRACKS AND SCRATCHES

A simple form of the renewal strings model was tested on plate datasets within the SSS. For the background star/galaxy process the local density was obtained by gridding the whole space into 40,000 boxes and counting the elements in each box. Improvements could be made through the use of a k-means or other density estimate. 1000 different angle settings were used, and 18000 different bins for the distance from the origin. Each data point was put in two bins (i.e. the line width was twice the distance separation). These values were obtained from simple geometric arguments. The number of bins for the distance from the origin was chosen based on the largest widths of the tracks which we were trying to detect. Then the angular variation was then chosen such that any significant length of any track will not be missed between two different angles.

A simple model of two hidden states was used, one corresponding to the background, another to the satellite track. The inter-point distribution for the satellite track was set to be an exponential distribution using the empirical mean from a training set including 30 different satellite tracks from low density plates (the resulting mean was 360 microns on the plate, corresponding to 24 arcsec on the sky). As stars and galaxies also appear along satellite tracks, this empirical mean was added to the mean of the background process to properly model the density along a satellite track in different circumstances. The transition probabilities were set approximately using prior knowledge about the number of satellite tracks etc. on the training plates, the number of objects in total and the number of objects per satellite track. This resulted in the transition matrix $P(X_t|X_{t-1})$ for $X = \{background,\ track\}$ of

$$\begin{pmatrix} 0.999998 & 0.04 \\ 2\times10^{-6} & 0.96 \end{pmatrix}$$

The initial prior probabilities were assumed to be the equilibrium probabilities of a Markov chain with these transitions.

Figures 7 and 8 gives a few examples of the results. The whole plate is a little under 350mm square, so some of these images are for very small regions. Figure 7b shows the results for a whole plate. Note these images also contain the results for diffraction spike and halo detection discussed in Sections 8 and 9. Stars or galaxies lying behind the path of a satellite track are also flagged, as the characteristics recorded for those objects will be affected by the existence of the track, and will therefore be unreliable.

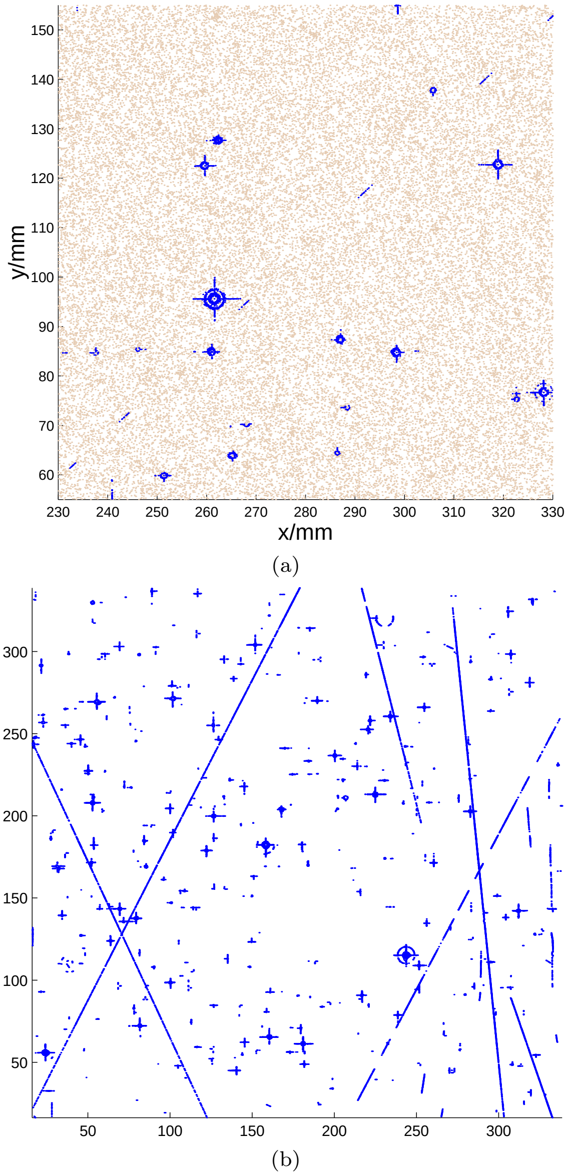

**Figure 7.** (a) An aeroplane track sloping from the bottom left to the top right: a faint dashed line caused by a flashing light is properly detected. (b) The detection results for the whole of UKJ159, including a number of satellite tracks or aeroplane tracks. One flashing aeroplane track traverses the right side of the plate.

### 7.1 Comparison of results with naive Hough transform

The simple Hough transform does a slightly different job from the renewal string approach, as it is designed to find lines which traverse the whole plate. If we wish to find line segments we have to do some post-processing of the results. The exact position of the tracks would still need separating from the other points in that Hough box. Even so we can assess how well the Hough transform can find lines which contain linear features.

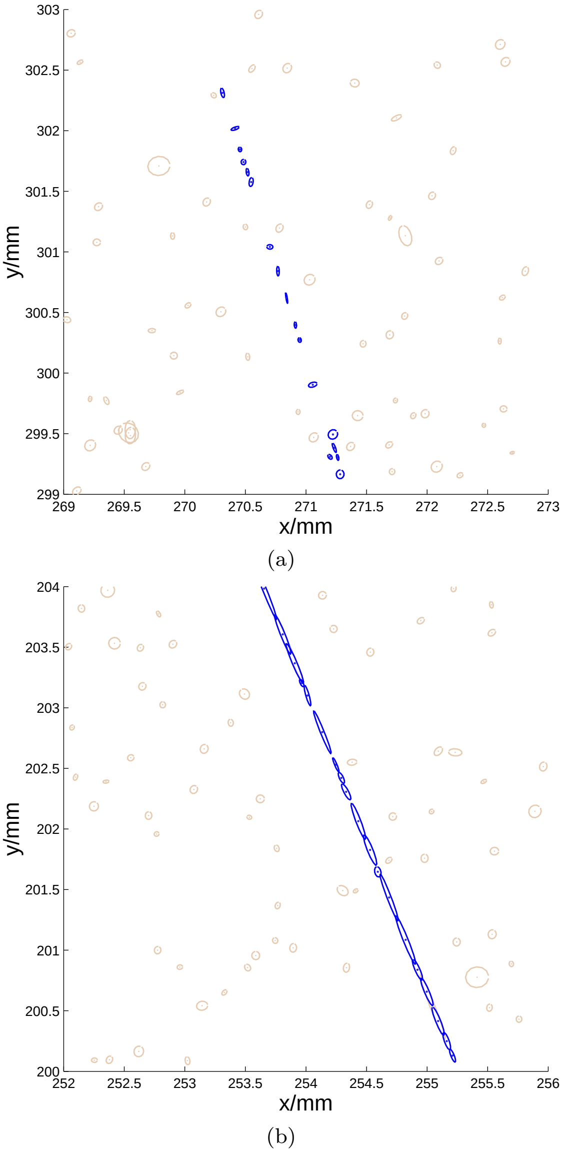

**Figure 8.** Detections along the parts of two satellite tracks on UKJ005. Other parts of these tracks were illustrated in Figure 1(a) the sparse track and (b) the dense track.

There are many decision functions which can be used with the Hough transform. For a useful comparison with the renewal string results, we look at the significance level which would be needed to detect each track that was detected with the renewal string method. We also look at how many other false positive tracks would also be detected for given significance levels. The number of angles and line widths considered were set to match the renewal string settings (1000 angles, 9000 different perpendicular distances)

Results for doing this on plate UKR002 are shown in Table 1. This plate has no satellite tracks that traverse the whole plate, but does have some smaller to medium size (a quarter of plate width) tracks and scratches. Each track was located in a semi-automated way, and diffraction spikes were ignored by removing all tracks within 1.5 degrees of the horizontal or vertical. The position and angle of each track was noted, and included in a track list. In general each track was noted once. However, where there was a large curvature to a track, more than one reference could have been included in the list. The points corresponding to the plate notes in the bottom left of the plate, and detections relating to a halo about a bright star were removed by hand. This left 35 tracks or scratches in the reference list.

For comparison purposes, we looked at all the listed tracks and calculated what significance level would be needed in order to detect the line containing that track with the Hough transform. The table shows the significance level required to detect the tracks along with the total number of tracks (true and false) which would have been detected by the Hough transform at various significance levels. These counts once again exclude Hough accumulators corresponding to lines within 1.5 degrees of the horizontal or vertical. The result was that a total of 968 different angles were considered. Accumulators with an expected count less than 12 were discarded as these are easily affected by isolated points.

Many of the tracks are picked up by the Hough transform for high significance levels. However some of the tracks are not even detectable at significance levels of 0.5 and smaller. Hence the renewal string approach is certainly increasing the detection rate compared with using the Hough transform alone. Furthermore the Hough transform produces large numbers of false positives even when only choosing very significant lines. The number of false positives on this plate is much greater than the theoretical number that should be found at the high significance levels. Some of these will be contributions from accumulators mapping to lines overlapping a track at a slight angle. However a dominant reason for the discrepancy is that global approaches like the Hough transform do not easily deal with variations in the background density; there is an assumption of homogeneity. If many stars are clustered in one location, then they can cause a significant contribution to a single Hough accumulator. As mentioned in section 6.1, if only the more significant detections are wanted then the Hough transform can be used to find proposal search lines, and then the renewal string approach allows the exact points in the track to be found along that line (if there are any). This can be a significant speed up over running a hidden Markov renewal process along every line. How many tracks would be missed depends on the significance level used, and in this circumstance can be estimated from Table 1. The lower the significance level, the more lines that would have to be checked, and hence the greater the computational cost.

## 8 DETECTIONS OF OPTICAL HALOS

Finding optical halos is possible using elliptical Hough transforms described in section 3.2. As the halos are almost circular, and centred near to bright stars it is only necessary to consider ellipses up to a certain radius, and in a limited number of centres, and with a limited amount of ellipticity. The possible centres are chosen to be near to bright stars.

To search around bright stars, a bright star set is needed. The measurement of the photographic magnitude of bright stars can be subject to quite large error. For this reason the measured size of the star is used as an indicator of its likelihood of producing halos (or diffraction spikes). We chose to consider all stars with a measured radius greater

| SIGLEV | DET | TOT | THEOR |
|---:|---:|---:|---:|
| 0.5 | 31 | $3.18 \times 10^6$ | $4.4 \times 10^6$ |
| 0.7 | 26 | $2.09 \times 10^6$ | $2.6 \times 10^6$ |
| 0.9 | 21 | $8.96 \times 10^5$ | $8.7 \times 10^5$ |
| 0.95 | 15 | $5.34 \times 10^5$ | $4.4 \times 10^5$ |
| 0.99 | 9 | $1.62 \times 10^5$ | $8.7 \times 10^4$ |
| 0.999 | 7 | 30147 | 8712 |
| $1 - 10^{-4}$ | 5 | 5903 | 871.2 |
| $1 - 10^{-5}$ | 4 | 1158 | 87.12 |
| $1 - 10^{-6}$ | 3 | 257 | 8.7 |
| $1 - 10^{-7}$ | 2 | 71 | 0.87 |
| $1 - 10^{-8}$ | 2 | 25 | 0.087 |
| $1 - 10^{-9}$ | 1 | 16 | 0.0087 |

**Table 1.** The number of the 35 tracks/scratches on UKR002 which would have been detected using the hough transform. SIGLEV gives the significance level used. DET gives the number of the tracks which would have been flagged at that significance level, TOT the total number of lines flagged as significant by the Hough transform, and THEOR the theoretical number of false positives for a homogeneous Poisson distribution. A significance level of $1 - 10^{-7}$ is needed to reduce the theoretical false positive detection rate to a suitably low level. Then only two of the tracks could have been detected, and in practice there would have been many false positives flagged.

than 200 microns. The star/galaxy classification flag can also be inaccurate for very bright stars, and so any object which is approximately circular is presumed stellar. We allowed a minimum ratio of 0.7 between the minor and major elliptical axes. This does result in some misclassification where stars in circular galaxies are presumed to be part of a halo around a star. Solutions to this problem are being investigated, including the possibility of building more accurate classifiers for stars and galaxies by training on the Sloan Digital Sky Survey classifications.

To detect the halos an elliptical Hough transform was used. The elliptical axes were presumed to be aligned along the x and y axes, and the ratio of the horizontal and vertical axes was varied from 0.8 to 1.2 in intervals of 0.05. The ellipse centres were chosen to be within 400 microns of the measured star centre, stepping in 80 micron intervals. The Hough transform searched through 200 different radii, each of width 40 micron. An allowance for the variation in background density of 1.1 times the measured density was used. The halos were expected to have a mean line density of 1 point every 380 microns over and above the background density, obtained from observations regarding the density of halos. Empirical estimates were used to calculate a prior probability of a randomly chosen ring about a bright star containing a halo of about 0.00003.

The objects were flagged when any ellipse containing them was found to have a posterior probability of greater than 0.5 of being a halo. The posterior probability of an object being part of a halo was assumed to be the greatest posterior probability of all the ellipses containing that object.

## 9 DETECTION OF DIFFRACTION SPIKES

Diffraction spikes occur around bright stars. They are linear features with many of the characteristics that other linear features have, and it is true that the application of the standard renewal string approach of the previous section will detect a large number of the diffraction spikes without any modification. This is because the renewal string approach is particularly suited to detection of short linear features as it is based on a model which allows the generation of short lines.

Despite the fact that diffraction spikes are also linear phenomena similar to scratches, there are significantly fewer degrees of freedom regarding where they lie. Hence they can be found with greater accuracy by focusing exclusively on lines passing through bright stars, and aligned almost horizontally and almost vertically to the image axes. This means that the renewal string methods described in the previous sections can be enhanced by restricting the renewal string algorithm to look only at near vertical and near horizontal lines in the region of a bright star. This enables the probability model to be tailored specifically to diffraction spikes rather than to all linear features.

The restricted renewal string approach was used in order to try to pinpoint the diffraction spike positions more accurately. The bright star set described in section 8 was used. 17 different angles in 0.3 degree gradations, and 17 different line positions at gradations of 13 micron were considered near to the axis aligned lines through the centre of the bright stars. These values appeared to cover the variation in the position and angle of the spikes without introducing excessive computational burden. In a similar way to the renewal string model, a hidden Markov renewal process was run along each of these lines. The main difference is that the process started at the closest point to the star centre, working out to the edge. The mean of the spike Poisson process was taken to be 190 microns, and the transition probabilities $P(X_t|X_{t-1})$ for $X = \{background,\ track\}$ were

$$\begin{pmatrix} 0.9992 & 0.23 \\ 0.0008 & 0.77 \end{pmatrix}$$

Due to the increased probability of a point near to the star being a part of a spike, the initial probabilities are no longer the equilibrium probabilities of the Markov chain. The initial probabilities $P(X_0)$ were set to be

$$\begin{pmatrix} 0.994 \\ 0.006 \end{pmatrix}$$

These probabilities were estimates based on the number of lines considered, the expected number of diffraction spikes which existed per star examined, the overlap of the lines, and the expected length of the lines. It is possible that these hand estimates could be enhanced using the expectation maximisation (EM) algorithm to obtain maximum likelihood parameter estimates. However that would increase the computational burden significantly for what would probably be small gain.

The usual renewal string inference (the forward backward equations of appendix A) was used to detect the positions of the diffraction spikes, again flagging for posterior probabilities greater than 0.5.

## 10 EVALUATION

The detections were evaluated by an astronomer (NCH), who looked through a printed version of the plate data for a

| | FP | FP% | FN | FN% | DET | TOT |
|---|---|---|---|---|---|---|
| Tracks | 60 | 0.7 | 14 | 0.0033 | 8539 | 429238 |
| Halos | 60 | 1.2 | 32 | 0.0075 | 5063 | 429238 |
| Spikes | 30 | 2.0 | 175 | 0.04 | 1482 | 429238 |

**Table 2.** Numbers of false positive (FP) and false negative (FN) records for satellite track/scratch detection, halo detection and diffraction spike detection on plate UKR001. False positive percentage expressed as percentage of total detections (DET); false negative percentage expressed as percentage of [total objects (TOT) - total detections (DET)].

whole plate (UKR001). The plate was split into 36 regions, each region being printed on an A3 sheet. These A3 sheets were examined closely for false negative and false positive detections, and the astronomer also commented on other aspects of the detection he felt notable. In this analysis features corresponding to small fibres were ignored. As the measured characteristics of true stars or galaxies along or very near a satellite track will be affected by the track, these objects should also be flagged.

A general summary of the results can be found in Table 2. All the major satellite tracks were found and the ends of the tracks were generally accurately delineated. All of the small scratches were properly identified, although one of them involved a significant bend. Figure 9 illustrates this. Some of the objects along the bend were improperly classified as real objects. A small number of small false positive linear detections were made. Some objects due to fibres on the plate were also picked up, although as expected the method was not designed for and is not ideally suited to their detection.

Another useful evaluation involves comparing the detections with cross-plate matches. Any objects which are due entirely to a satellite track or scratch will not have a corresponding record in other data taken at different epochs or different wavelengths. If we presume that any objects which do pair across different surveys are real astronomical objects or optical artefacts, then we can make an assessment of how many objects are being flagged which are definitely not due to a track or scratch.

Of the 3.1 million objects on the 8 plates, 10029 objects were located by the renewal string algorithm as part of a scratch or track. Of these only 552 (5%) were paired across different surveys, indicating they were true astronomical objects or related to optical artefacts. Nearly all of these were stars and galaxies lying along the line of the satellite tracks, which should be flagged as problematic anyway.

Some examples of the tracks found can be seen in Figure 10. Figure 11a shows a number of points which were flagged as spurious by the renewal string approach. This is located on UKR001 around $RA = 2:34:52$, $DEC = -86:32:16$. The astronomer marked this up as a false positive

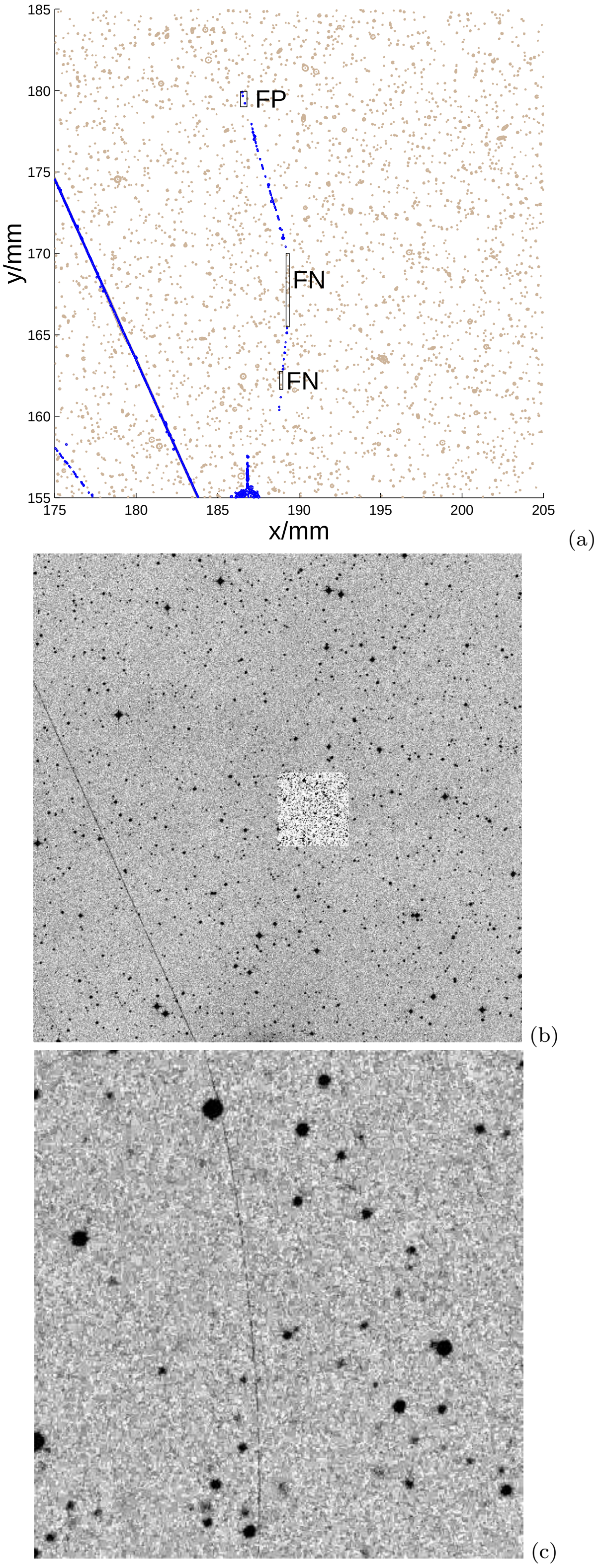

**Figure 9.** (a) False positives (FP) and false negatives (FN) for detections along a very faint highly curved scratch on plate UKR001. This is the only significant source of false negatives for scratch/track detection that the astronomers found on this plate (the others were isolated points at the end of a scratch). The scratch is not easily seen in the corresponding image (b), but can be seen in the detail (c) of the brightened region of (b).

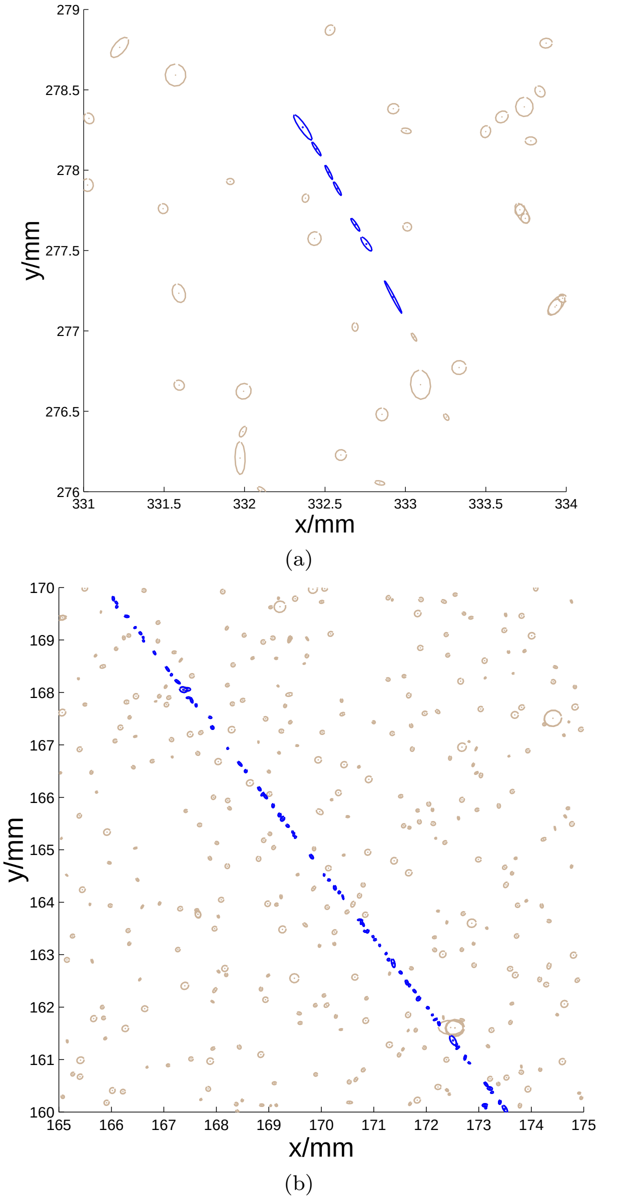

(a)

(b)

**Figure 10.** (a) A very short scratch which was detected. (b) A typical part of a large satellite track.

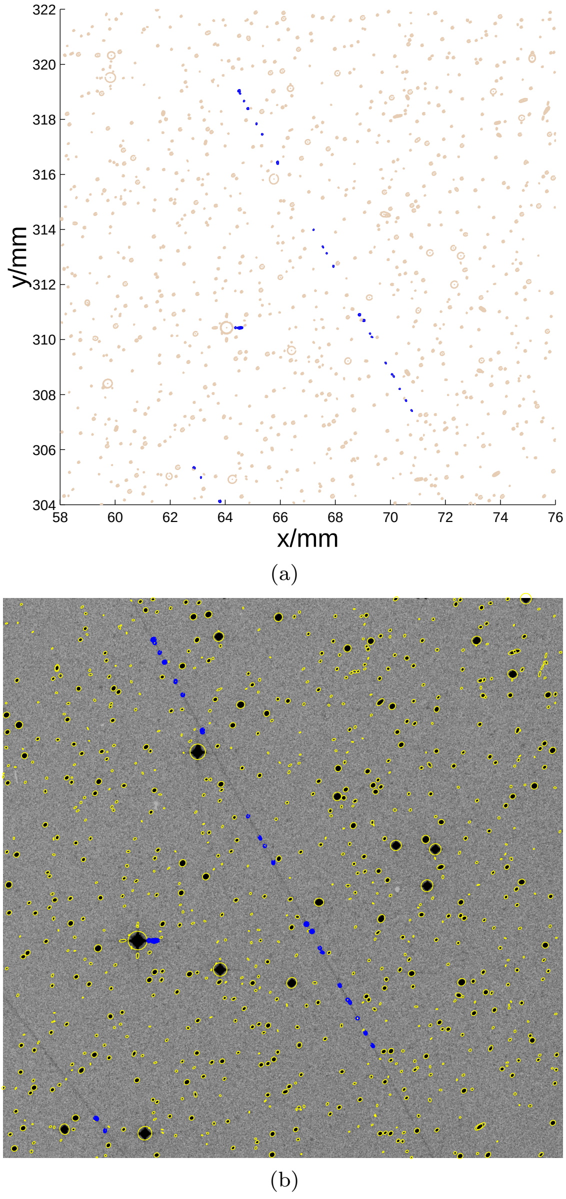

(a)

(b)

**Figure 11.** (a) A set of detections on UKR001 which were marked up as false positives by the astronomers. (b) A look at the image shows the points are in fact part of a faint track.

detection, as it did seem to look like stars and galaxies which just happened to be aligned. However when looking at the image (Figure 11b), it is clear that these points are aligned along a very faint track. For most of the track the image is too faint to produce any spurious records. However for this short section some spurious records do occur. The fact that this is the case can be seen by looking at the corresponding image part in the overlap with plate UKJ003, where no such objects are recorded.

Again on UKR001, the halos of the bright stars were picked up accurately. There were some false positives due to the other local features being misinterpreted as halos. For example a high density cluster might contribute to a high Hough accumulator count for a given ellipse, causing other points in that ellipse to also be classified inaccurately. In general though because the halo detection is a Hough approach, the density variation along the path of the larger halos is not taken into account, and this can cause problems such as these. From Table 2, it can be seen that the number of false positives is still a small proportion of the total detections [3].

Most, but not all of the diffraction spikes were detected. In general we presume that a diffraction spike will need to contain about 4 objects before we would expect this algorithm to detect it. The most common failures were false negatives. The majority of these were diffraction spikes on stars which were only just bright enough to have spikes,

[3] Classifications are only illustrated for the deblended objects. Some of the objects on these plots can be seen to be larger parent objects which have a number of deblended children.

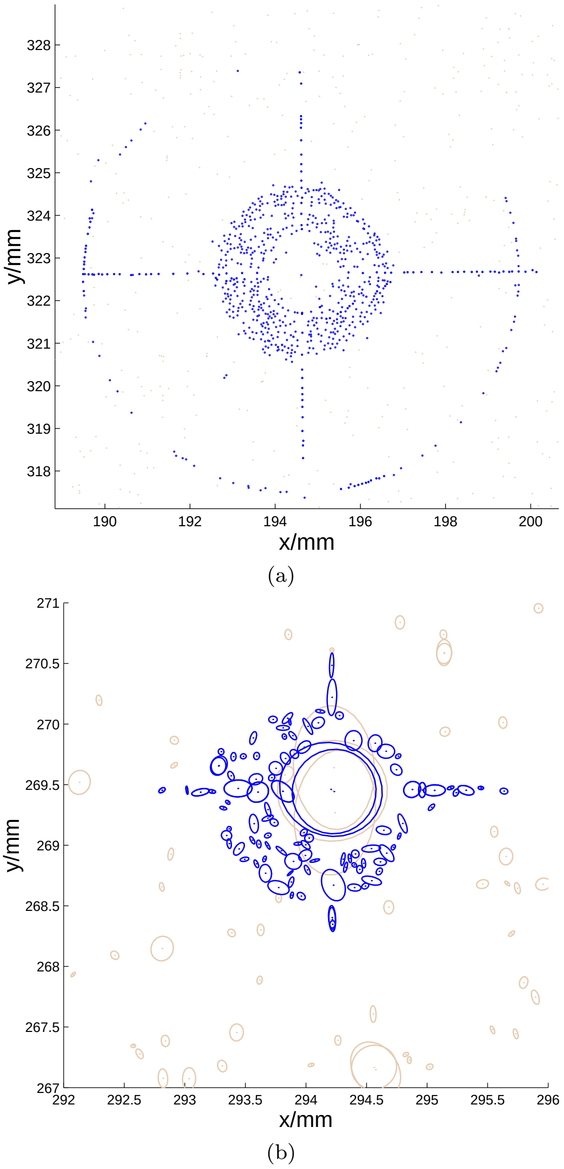

(a)

(b)

**Figure 12.** (a) A set of halos and diffraction spikes around a bright star on UKR002 at RA= 23 : 52 : 7, DEC= −82 : 01 : 14. (b) One of many medium-bright stars on UKR002 with associated halo and diffraction spikes.

where the spikes were represented as four objects. Some were failures to recognise the true extent of a diffraction spike. Even so the number of false negatives was relatively small. There were also some false positives due to overrun of the diffraction spike detection beyond the end of the spike, and other effects such as two adjacent bright stars whose halos and diffraction spikes interacted with one another. Again the number of false positives was a small percentage of the overall detections.

Examples of the halo and diffraction spike detection can be found in Figure 12. These show one bright (a) and one less bright (b) star, and their associated halos and diffraction spikes. Example detections on a whole plate can be seen in Figure 7b.

In general we are getting good detection rates for all three problem features. This will make a major difference to the reduction in spurious data problems in the catalogue.

## 11 DISCUSSION

Renewal Strings have certainly aided the process of detection of spurious objects in astronomical data: given very large amounts of data only a small number of detections were made, most of which were correct. The form of the model allows the use of the hidden Markov models and renewal processes, resulting in a model that is efficient even for huge datasets. It has been run all the plates of the SSS data (over 3000 in total), providing a valuable resource to astronomers.

Renewal strings are a practical, probabilistic approach to a large problem requiring high accuracy. Renewal strings go beyond a local Hough transform method to a general approach for detecting line segments within large amounts of other data. Slightly curved lines are also detectable as a set of locally linear parts.

Hough transform approaches were also suitable for halo detection. Some of the false positives reflected the difficulty that Hough approaches have in dealing with local density variations. One way of improving the current approach would use renewal strings around the arc of the halo in much the same way that is currently used for straight lines. This would allow the local densities to be modelled more accurately.

The renewal string approach has also been adapted for diffraction spike detection, and shows promising results. One noticeable improvement would involve the introduction of prior information regarding the length of the diffraction spike depending on the brightness of the star. However inaccuracies in the measured star brightness, and significant variations in spike length depending on the position of the star, or density and colour of the plate, have made this a nontrivial task. Despite this the current method is providing accurate detection results, and enables the recognition of the vast majority of diffraction spike objects with relatively few false positives.

The renewal string approach shows clear benefits over Hough approaches, and has proven a highly effective method for detection of spurious data in the SuperCOSMOS Sky Survey. The results of the method will reduce the problem of spurious data in these surveys to insignificant levels. Furthermore the technique is general and can be adapted for use in future sky surveys. The techniques will also be useful in fully digital sky surveys. These techniques are particularly suitable for detection of the shorter satellite and aeroplane tracks which can be found in many digital surveys.

The results of the application of this approach to the SuperCOSMOS Sky Survey will be made available in a forthcoming new release (Hambly et al., 2003, in preparation) of the survey data. This new release will incorporate several new data enhancements (eg. to proper motions, photometric calibration scales and source pairing) along with enhancements to user access. The existing standard SSS distribution is available at `http://www-wfau.roe.ac.uk/sss/`.

*Acknowledgements*

This work is part of a project funded by the University of Edinburgh. The authors also thank IBM for the generous provision of the P-Series machine Blue Dwarf to the School of Informatics, Edinburgh through the Shared University Research Programme. This machine was used for some of the runs on the SuperCOSMOS Sky Survey data. The first author would like to thank Microsoft Research for fellowship funding for the final stages of this work.

## APPENDIX A: INFERENCE IN HIDDEN MARKOV MODELS

In this Appendix the update equations for a hidden Markov model are given. For more details see e.g. Rabiner (1989); Castillo et al. (1997). Suppose the number of states for the HMM is denoted by $M$, the latent class variables denoted by $X$ and the visible variables by $Y$. Subscripts are used to denote the time index from 0 to $T$. Then the state transition matrix at time $i$ is $P(X_{i+1}|X_i)$. The output distribution is $P(Y_i|X_i)$, and the initial class probabilities are $P(X_0)$. The update equations for inference in a hidden Markov model consists of a backward and a forward pass. We presume that all the $Y_i$ are given. The backward pass propagates the data likelihood back through time. Once that is complete, the forward pass propagates the prior information forward through time.

Let $\lambda_i(X_i) = P(Y_{i-}|X_i)$ denote the backward message at time $i$ for each class (1 to $M$) taken by $X_i$. Here $Y_{i-}$ denotes the set of all of the observable values for times after and including time $i$. Likewise $\rho_i(X_i) \propto P(Y_{i+}, X_i)$ is the forward message at time $i$, where $Y_{i+}$ denotes the set of all of the observable values for times before time $i$. Then we can update $\lambda$ by using the initialisation $\lambda_T(X_T) = 1 \ \forall X_T$ and then applying the recursive formula

$$\lambda_i = P(Y_i|X_i) \sum_{X_{i+1}} P(X_{i+1}|X_i)\lambda(X_{i+1}). \qquad \text{(A1)}$$

Likewise we initialise $\rho_i(X_0) = P(X_0)$ and apply the recursive formula

$$\rho_i(X_i) = \sum_{X_{i-1}} P(X_i|X_{i-1})\rho_i(X_{i-1})P(Y_{i-1}|X_{i-1}) \qquad \text{(A2)}$$

The final marginal posterior probabilities (beliefs) are given by

$$P(X_i|\{Y_j \ \forall j\}) = \alpha\lambda_i(X_i)\rho_i(X_i) \qquad \text{(A3)}$$

with $\alpha$ a normalisation constant.

The beliefs can be calculated in time linear in the number of nodes.

## REFERENCES

Ballard D., 1981, IEEE Trans. on Pattern Analysis and Machine Intelligence, 13, 111

Banday A., Zaroubi S., Bartelman M., eds, 2001, Mining the Sky. ESO Astrophysics Symposia XV

Bengio Y., Frasconi P., 1996, IEEE Transactions on Neural Networks, 7, 1231

Bock D.-J., Large M., Sadler E., 1999, AJ, 117, 1578

Brown M., Taylor A., Hambly N., Dye S., 2002, MNRAS, 333, 501

Castillo E., Gutierrez J. M., Hadi A. S., 1997, Expert Systems and Probabilistic Network Models. Springer, New York

Chen H., Meer P. L., Tyler D. E., 2001, IEEE Conference on Computer Vision and Pattern Recognition, 1069

Cheselka M., 1999, Astronomical Data Analysis Software and Systems VIII, ASP Conference Series, 172, 349.

Fischler M. A., Bolles R. C., 1981, Communications of the ACM, 24, 381

Hambly N., Miller L., MacGillivray H., Herd J., Cormack W., 1998, MNRAS, 298, 897

Hambly N. C., et al H. T. M., 2001, Monthly Notices of the Royal Astronomical Society, 326, 1279

Hambly N. C., Irwin M. J., MacGillivray H. T., 2001, Monthly Notices of the Royal Astronomical Society, 326, 1295

Hastie T., Stuetzle W., 1989, Journal of the American Statistical Association, 84, 502

Hough P., 1959, International Conference on High Energy Accelerators and Instrumentation

Kiryati N., Bruckstein A. M., 1992, IEEE PAMI, 14, 495

Kiryati N., Eldar Y., Bruckstein A. M., 1991, Pattern Recognition, 24, 303

Oppenheimer B., Hambly N., Digby A., Hodgkin S., Saumon D., 2001, Science, 292, 698

Otterpohl J., Haynes J., Emmert-Streib F., Vetter G., 2000, Journal of Physiology, 94, 555

Paciesas W., et al., 1999, ApJSS, 122, 465

Pearl J., 1988, Probabilistic Reasoning in Intelligent Systems: Networks of Plausible Inference. Morgan Kaufmann

Rabiner L. R., 1989, Proceddings of the IEEE, 77, 257

Scott S. L., Smyth P., 2003, The Markov Modulated Poisson Process and Markov Poisson Cascade with Applications to Web Traffic Modeling, To appear in Bayesian Statistics 7

Storkey A. J., Hambly N. C., Williams C., Mann R. G., 2003, in Uncertainty in Artificial Intelligence: Proceedings of the Nineteenth Conference (UAI-2003) , 559

Vandame B., 2001, in Mining the Sky, Proceedings of the MPA/ESO/MPE Workshop, 595